MODELING OF THE ELASTIC-PLASTIC BEHAVIOR OF ADHESIVE FILMS USED IN COMPOSITE BONDED JOINTS OF AIRCRAFT STRUCTURES

J. Maurice[1,2*], J-Y. Cognard[2], R. Créac'hcadec[2], P. Davies[3], S. Mahdi[1]

[1]*Airbus Operations S.A.S, Toulouse, France*
[2]*LBMS ENSTA-Bretagne/ENIB/UBO, ENSTA-Bretagne, Brest France*
[3] *IFREMER Materials and Structure group, centre de Brest, Plouzané, France*
** julien.maurice@airbus.com, julien.maurice@ensta-bretagne.fr*

Keywords: Adhesive bonding, 3D Elastic-plastic behavior, Modified Arcan test

Abstract

Adhesive bonding has increasingly gained in importance in the design of commercial aircraft structures over the last 50 years and is now widely used in primary composite parts such as fuselage and wings. In order to optimize bonded joints, accurate modeling of the adhesive behavior and dedicated sizing approaches have to be developed. This study first focuses on the characterization of the 3D elastic-plastic behavior of different adhesive films using a modified Arcan device. A model taking into account hydrostatic stress dependency and non-associated formalism has been identified using these experimental results. Comparisons between numerical and experimental results considering composite single-lap joint tests and bonded stringers representative of a composite fuselage are then presented and analyzed.

1 Introduction

1.1 Context

Characterization of adhesive materials and modeling of the behavior of composite structural bonded parts remains a challenging task. Adhesives, as polymeric materials, show a complex 3D behavior in the range of loads and conditions encountered by aircraft structures. In particular, their elastic-plastic behavior is known to be dependent on the hydrostatic stress invariant [1-4]. Thus, dedicated constitutive laws and experimental strategies have to be developed.
Experimentally, the main difficulties are:

- the thin thickness of the aeronautical adhesive films (typically from 100 µm up to 200 µm) that leads to measurements of very small displacements.
- Experimental characterization has to cover a wide range of loads in order to accurately describe the hydrostatic stress dependency.
- Most of the existing normalized tests only enable one type of load to be applied. Different test configurations must therefore be used [4] except for the tension-torsion butt joint, for which appropriate test machines are not common. In addition, most of the joint specimens suffer from edge effects (stress

concentrations) which can lead to premature crack-onset and thus biased characterization [5,6].

In this study, we used a modified Arcan device [3]. This test enables a large experimental database to be obtained under a wide range of loads, using a unique bonded specimen design which limits edge effects. A simplified inverse identification method, developed previously [7], has been applied to characterize four adhesive films. Validation of this identification is then proposed and analyses of application cases are carried out.

1.2 Materials and process

Four aeronautical adhesive films, consisting of two resins (A and B) with two types of carriers (Knit or Mat) have been studied. Although the initial thickness varies slightly from one manufacturer to another, the films considered here are almost 100 µm and 200 µm thick respectively for the Mat and the Knit configurations. For the aluminum Arcan specimen surface preparation consisted of an anodization, whereas for the composite specimens, peel-ply or grid blasting process, following aeronautical specifications, were used. All specimens were bonded in an autoclave.

1.3 Modified Arcan Test

The modified Arcan device is presented in figure 1.a. It enables the bonded specimen to be loaded at different load ratios defined by angle γ. The test set-up is presented in figure 1.b. 3D digital image correlation is used to measure the relative displacements of the substrates in both the normal (N) and the tangential (T) directions.

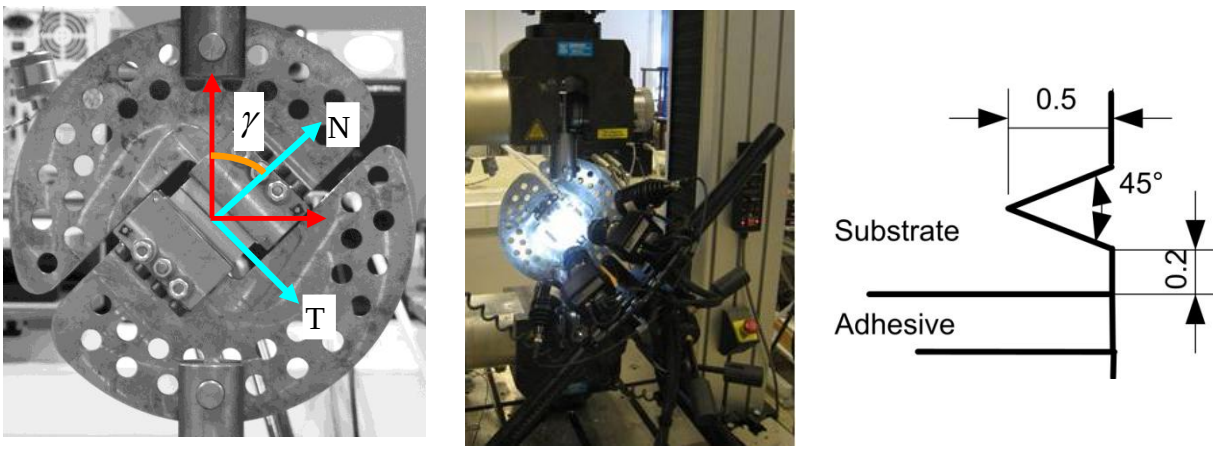

(a) (b) (c)

Figure 1. Modified Arcan test: device (a), set-up (b) and specimen geometry (c)

Here the bonded specimens were made of aluminum with a special assembly design including machined “beaks”, near the bonded surface, manufactured as presented in figure 1.c. This enables edge effects to be limited and having the highest stress amplitudes in the center of the bonded joint, which leads to very small scatter in the experimental results. Examples of experimental results for the A/Mat adhesive are presented in figures 2 and 3. For mixed loads (γ=30°, 45°, 75° or 135°) the responses in the normal and tangential directions have been separated since a ratio of about 1/10 is observed. Whatever the ratio, good repeatability can be observed, the very small displacements encountered in the normal direction should be noted.

2 Identification of the model

2.1 Mahnken-Schlimmer model and identification strategy

The model proposed by Schlimmer [2] has been chosen following previous studies [3,7]. The equations defining the constitutive law are summarized in table 1.
σ_{VM} is the von Mises equivalent stress and p the hydrostatic stress component defined according to the decomposition of the stress tensor $\underline{\underline{\sigma}}$ into the deviatoric part ($\underline{\underline{S}}$) and the hydrostatic stress (Equation 1.).

$$\underline{\underline{\sigma}} = \underline{\underline{S}} + pI_d \qquad \sigma_{VM} = \sqrt{\frac{3}{2}\underline{\underline{S}} : \underline{\underline{S}}} \qquad p = \frac{1}{3}tr(\underline{\underline{\sigma}}) \tag{1}$$

Yield surface	$F^{MS} = \sqrt{\sigma_{VM}^2 + a_1 Y_0 p + a_2 p^2} - Y$
Hardening	$Y = Y_0 + q(1 - e^{-be_v}) + He_v$
Internal strain-like variable	$\dot{e}_v Y_0 = \underline{\underline{\sigma}} : \underline{\underline{\dot{\varepsilon}}}^{pl}$
Flow rule / inelastic straining	$G^{MS} = \sqrt{\sigma_{VM}^2 + a_2^* p^2} - Y$ $d\underline{\underline{\varepsilon}}^p = d\lambda \frac{\partial G}{\partial \underline{\underline{\sigma}}}$

Table 1: Mahnken-Schlimmer model

The model is thus, by this a-priori definition, chosen non-associated, since the flow rule and the yield function may not be the same.

In order to deal with the non-uniform stress state (according to FEA under elastic assumptions, [3]) within the adhesive layer in the modified Arcan specimens used, a simplified inverse identification has been developed. The process consists of three steps using the modified Arcan results in order to identify the parameters of the model:

- Identification of the initial yield surface (Y_0, a_1 and a_2), using linear elastic simulations.
- Identification of the hardening function (q, b and H), using inverse identification and the experimental results in shear (γ=90°).
- Identification of the flow rule parameter (a_2*), using inverse identification and the results in tension-shear (γ=45°) or compression-shear (γ=135°).

More details on this procedure and results for other adhesives than those considered here can be found in [7].

2.2 Example of experimental results and identification

The identification has been performed for the adhesive films considered. Comparisons

between the experimental and FEA results for the different ratios used are presented in figure 2. The results show an overall good correlation between the model and the experimental results.

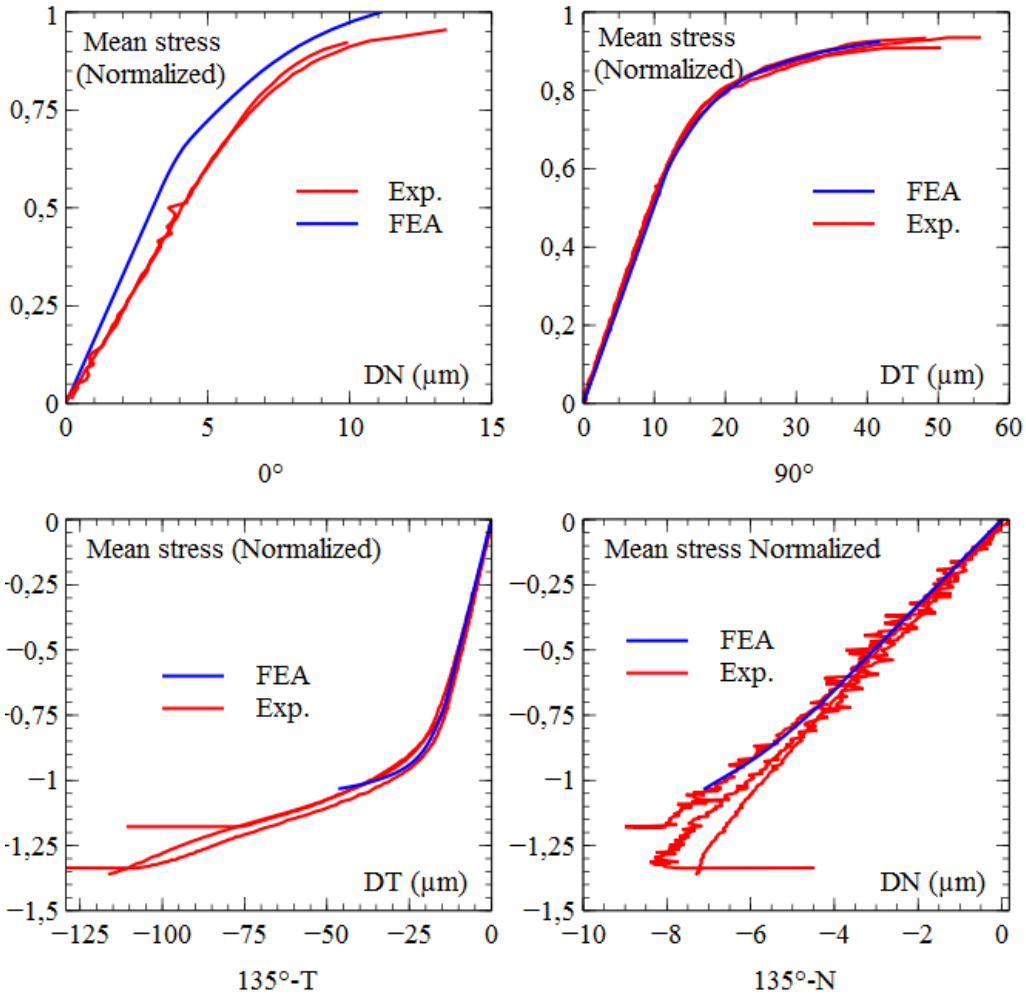

Figure 2. Identification of the MS model (normalized results): Experiments vs. FE results.

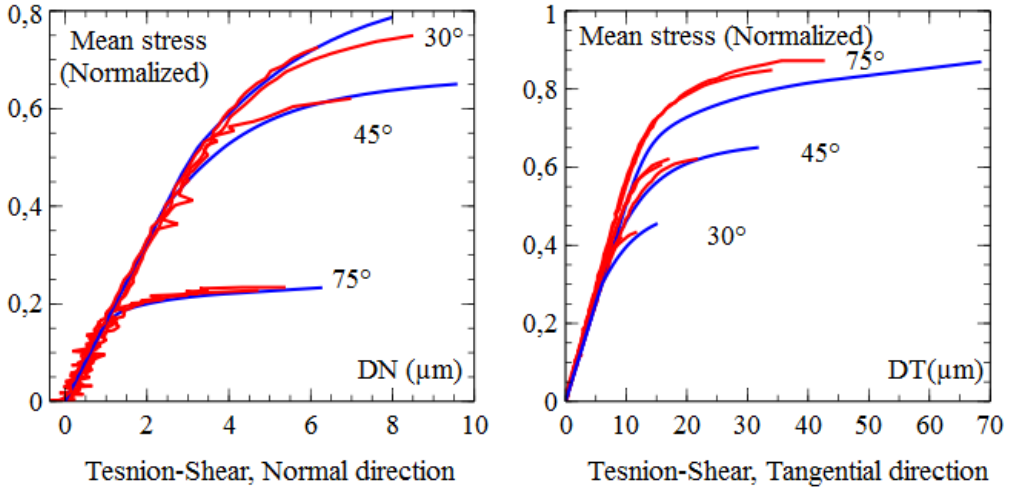

Figure 3. Validation of the identified parameter set (normalized results): Experiments vs. FE results.

3 Validation and comparisons

3.1 Modified Arcan results: complementary loads

In order to validate the identification, a first validation step was realized by considering other load ratios with the modified Arcan test. For example, experimental tests in tension-shear with γ values of 30°, 45° and 75° were performed and compared with FEA predictions. These results are presented in figure 3. Once again, a good global correlation with the model can be noted.

3.2 Comparison of the different adhesive films: Yield Surfaces

The good versatility of the model and the identification process proposed enable precise comparisons of different adhesives over a wide range of considered loads. In particular the comparison of the yield surfaces of the different films studied, eventually with different thickness – but at a constant strain rate – is of particular interest (figure 4). For the adhesive film A, there is a clear difference between the mat and the knit configurations whatever the stress path considered. Whereas for film B, the main differences appear in the tension-shear domain. It seems also that the initial bondline thickness within the Arcan specimen influences the results, since for the B/knit adhesive, results obtained for 95 µm and 183 µm thick bonded layers clearly differ. On the other hand, the yield surfaces for the B/Mat 95µm thick and B/knit 95 µm are relatively close.

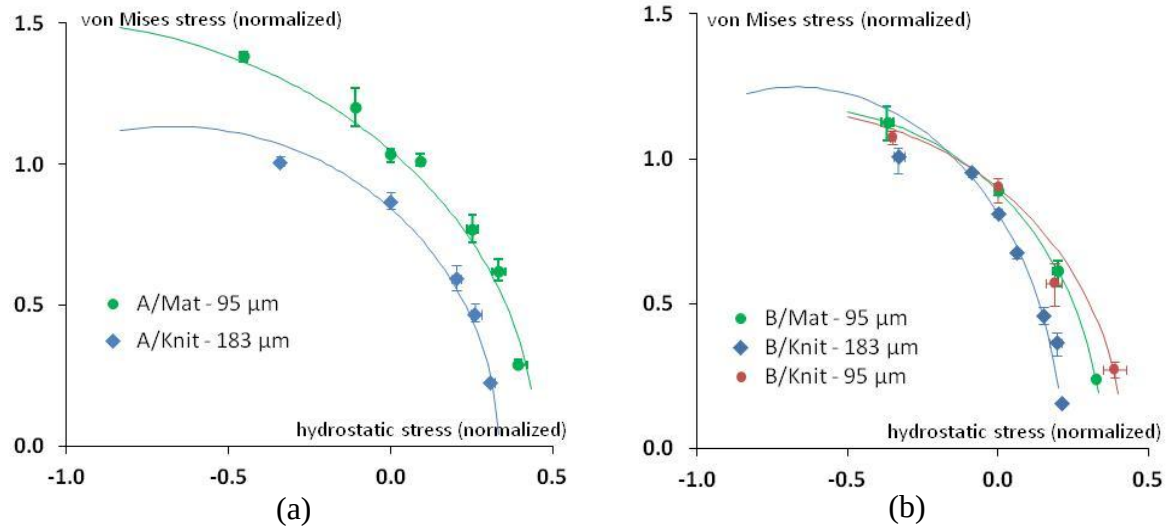

Figure 4. Comparisons between different adhesive films (normalized results): (a) A and (b) B

4 Applications

Applications of the identified model have been performed and results were compared to experimental results for CFRP single lap joint and omega stringers representative of fuselage configurations.

4.1 Single lap joint

The single lap bonded joint specimen is a common shear strength test. The configuration used here is presented in figure 5. The bonded area was 12 mm long and 25 mm wide while the total length of the specimen was 200 mm. Substrates were 2 mm thick and made of unidirectional CFRP plies. Three modes of curing (co-bonding, co-curing with adhesive and secondary bonding) were considered with 5 specimens of each.

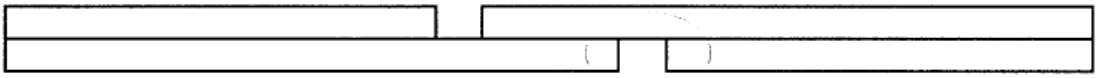

Figure 5. Single lap-joint test: schematic configuration

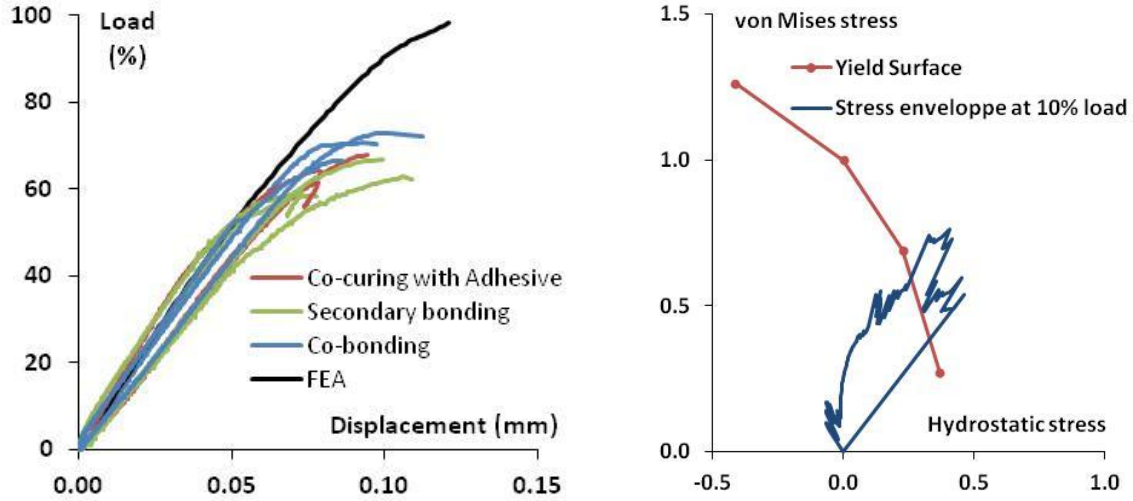

Figure 6. Normalized results: (a) FEA vs. Experimental results and (b) Stress envelope vs. yield surface

Different failure modes were observed: mixed adhesive/cohesive failure or cohesive within the first ply adjacent to the bonded layer. A full 3D elastic-plastic FE analysis with a relatively fine mesh (size of 10 µm within the bonded layer) was carried out. Comparisons between FEA predictions using the identified model and experimental results (figure 6a) show that the experimental failures occur at a very low load level; before the macroscopic inelastic behavior may develop. This is explained by stress concentrations, at high hydrostatic stress that appear at the ends of the bonded length. Figure 6b plots the external envelope of the stress state for all the integration points within the adhesive area at 10 % of the failure load. It is clear that the yield stress has been passed at this load. Despite being localized at the ends of the bonded layer, failure of this area, mainly in a tension-shear mode, will occur well before inelastic behavior in shear can develop due to the dependence on the hydrostatic stress.

4.2 Omega stringer

30 mm width coupons were extracted from a flat panel representative of the A350 XWB fuselage. Skin and stringer were made of quasi isotropic laminate composite, approximately 2 mm thick and co-bonded. These coupons were tested in 4 point bending (figure 7a) considering different configurations and lengths between the support points. The force vs. displacement curves obtained for one of them are presented in figure 8a. Instrumentation of

the specimens included strain gauges to validate the loading symmetry, acoustic emission, and four cameras (2D digital correlation) used to precisely observe the bonded areas at the four stringer ends (figure 7b). For each load case, three to five tests were realized. A simplified 3D analysis considering only 1/100 of the width of the coupons but with a refined mesh size (5µm) to model the stress distribution within the adhesive layer was used. The comparison between FE results and experiments is presented in figure 8a.

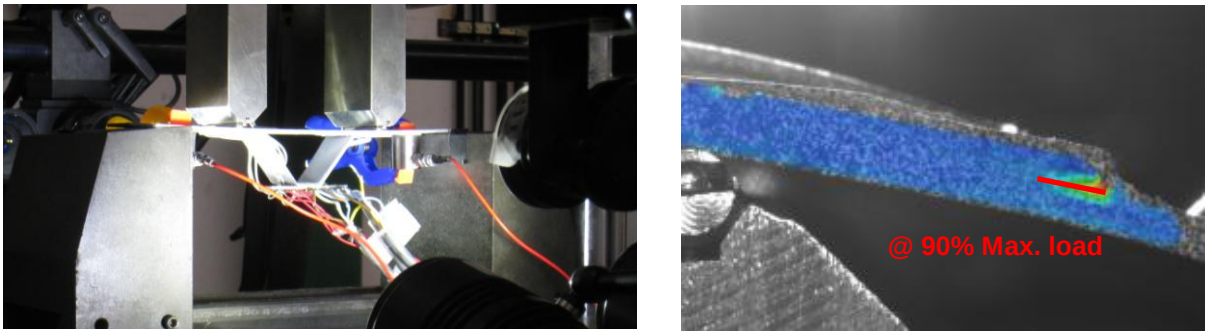

(a) (b)

Figure 7. Experimental set-up (a) and detailed analysis of a stringer end by 2D digital image correlation

Analyses of the experimental results show that different events occur before crack onset and propagation up to failure. The main one is a crack (horizontal) in the bonded layer that occurs at 90% of the failure load almost simultaneously for both stringer feet, near the spew fillet. FE analysis of the stress state within the external spew fillet and the whole adhesive layer corresponds to this observation (figure 8b). The stress state in the spew fillet is expected to be the most critical; according to the results presented in section 2, the inelastic behavior in tension-shear remains restricted. The rest of the adhesive is loaded in shear or compression-shear but the areas in tension-shear are the most critical due to the hydrostatic stress dependency.

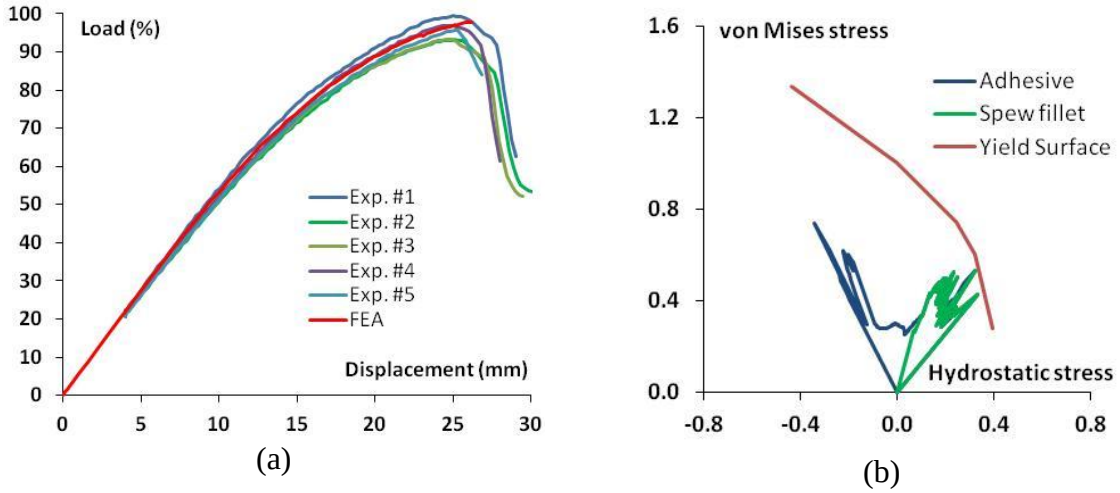

(a) (b)

Figure 8. (a) FEA vs. Experimental results. (b) Stress envelope vs. yield surface

5 Conclusions

The modified Arcan test allows a large database to be produced, with low scatter, and thus enables an advanced 3D constitutive law to be identified and challenged over a wide range of combined loads. For a good description of the adhesive behavior, hydrostatic stress dependency and non-associated formalism have to be taken into account. Precise comparisons between different adhesives require such a large spectra of loads to be covered. Indeed, for the adhesives considered in this study, the main differences occur in the tension domain, which is not the preferred mode of loading nor the easiest to characterize, but is the most critical as demonstrated for the single lap joint and the omega coupon stringer cases. The overall approach described here should thus allow the development of stress criteria taking into account the von Mises and hydrostatic stress components for detailed sizing approaches.

Acknowledgements

The authors wish to acknowledge Laurent Kerneis from LBMS-ENSTA Bretagne for his collaboration on the manufacturing of the bonded assemblies.

References

[1] Adams R.D., Comyn J., Wake W.C., *Structural Adhesive Joints in Engineering*, Chapman & Hall, London, (1997)

[2] Mahnken R., Schlimmer M., Simulation of strength difference in elasto-plasticity for adhesive materials, *International Journal of Numerical Methods in Engineering*, **63**, pp. 1461-1477 (2005)

[3] Cognard J.Y., Davies P., Sohier L., Créac'hcadec R., A study of the non-linear behavior of adhesively-bonded composite assemblies, *Composite Structures*, **76**, pp. 34-46 (2006).

[4] Wang C.H., Chalkley P., Plastic yielding of a film adhesive under multiaxial stresses, *International Journal of Adhesion and Adhesives*, **20**, pp.155-164 (2000).

[5] Dean G., Crocker L., Read B., Wright L., Prediction of deformation and failure of rubber-toughened adhesive joints, *International Journal of Adhesion and Adhesives*, **24**, pp. 295-306 (2004).

[6] Cognard J.Y., Créac'hcadec R., Sohier L., Davies P., Analysis of the non linear behaviour of adhesives in bonded assemblies. Comparison of TAST and ARCAN tests, *International Journal of Adhesion and Adhesives*, **28**, pp. 393-404 (2008).

[7] Maurice J., Cognard J.Y., Créac'hcadec R., Davies P., Sohier L., Mahdi S., Characterization and modeling of the 3D elastic-plastic behavior of an adhesively bonded joint under monotonic tension/compression-shear loads: influence of three cure cycles, *Journal of Adhesion Science and Technology*, under press (2012).